

Valley Splitting and Valley Dependent Inter-Landau-Level Optical Transitions in Monolayer MoS₂ Quantum Hall Systems

Rui-Lin Chu¹, Xiao Li², Sanfeng Wu³, Qian Niu², Wang Yao⁴, Xiaodong Xu^{3,5}, and Chuanwei Zhang^{1*}

¹ *Department of Physics, the University of Texas at Dallas, Richardson, TX 75080 USA*

² *Department of Physics, The University of Texas at Austin, Austin, Texas 78712, USA*

³ *Department of Physics, University of Washington, Seattle, Washington, USA*

⁴ *Department of Physics and Center of Theoretical and Computational Physics, University of Hong Kong, Hong Kong, China and*

⁵ *Department of Material Science and Engineering, University of Washington, Seattle, Washington, USA*

The valley dependent optical selection rules in recently discovered monolayer group-VI transition metal dichalcogenides (TMDs) make possible optical control of valley polarization, a crucial step towards valleytronic applications. However, in the presence of Landau level (LL) quantization such selection rules are taken over by selection rules between the LLs, which are not necessarily valley contrasting. Using MoS₂ as an example we show that the spatial inversion-symmetry breaking results in unusual valley dependent inter-LL selection rules, which is controlled by the sign of the magnetic field and directly locks polarization to valley. We find a systematic valley splitting for all LLs in the quantum Hall regime, whose magnitude is linearly proportional to the magnetic field and in comparable with the LL spacing. Consequently, unique plateau structures are found in the optical Hall conductivity, which can be measured by the magneto-optical Faraday rotations.

PACS numbers: 73.43.-f, 71.70.Di, 78.55.Ap, 71.35.Ji

Optical properties of two-dimensional (2D) charge carrier systems such as 2D electron gases (2DEG), graphene, and topological insulators are important for studying their underlying charge carrier properties and future applications in optoelectronics¹⁻¹². Generally, the charge carrier dynamics can be strikingly different with and without a magnetic field, as evidenced by the celebrated example of quantum Hall effect (QHE). In the quantum Hall regime, an external large magnetic field produces a series of Landau levels (LLs) with discrete energies and the optical transitions occur only between appropriate LLs following certain selection rules. In the past few decades, such selection rules and relevant optical phenomena have been intensively studied in various magneto-optical measurements^{1-6,8,9,11-15}.

Monolayers of MoS₂ and other group-VI transition-metal dichalcogenides (TMDs) represent a new family of 2D materials beyond graphene. Because of their coupled spin and valley physics and large band gap, monolayer TMDs have become exciting platforms for exploring novel valleytronic and optoelectronic applications¹⁶⁻²². Recently, the optical properties of TMDs in zero magnetic field have been widely studied in many experiments²¹⁻²⁴. However, the counterpart in a finite magnetic field has not been well explored.

In this work, we study the optical properties of monolayer MoS₂ quantum Hall systems with a large magnetic field. With a zero magnetic field, it is known that monolayer MoS₂ and graphene share similar valley contrasting physics, i.e., the circular polarizations (σ_+ , σ_-) are locked with two inequivalent valleys K and K' due to the opposite orbital helicity of two valleys²⁵⁻²⁸. However, with a large magnetic field in graphene, the polarization is no longer associated with the valley degree of freedom

because the transitions are between LLs, whose selection rules allow transitions in both polarizations (σ_+ and σ_-) at both valleys (K and K'), as observed in many magneto-optical measurements^{6,8,13-15}. Furthermore, such inter-LL selection rules in graphene are the same as 2DEG with large band gaps (e.g., GaAs quantum wells), where valleys do not even exist¹⁻⁵. These known results naturally indicate that the optical responses of monolayer MoS₂ in the quantum Hall region should also be valley independent.

Surprisingly, we find this is not the case for monolayer MoS₂, where the polarization selection rules for the inter-LL transitions are still valley dependent. More interestingly, the selection rules are controlled by the sign of the magnetic field, i.e., the valley index in the selection rules can be flipped by reversing the sign of the magnetic field, which is fundamentally different from the zero magnetic field case, where the polarization-valley locking is fixed. We also show that optical transitions in this system are made more unusual by a systematic valley splitting for all LLs, whose magnitude is linear against the magnetic field and is comparable with the LL spacing. The valley-polarization selection rules and valley splitting lead to a series of spin-valley polarized transitions between LLs as well as unique plateau structures in the optical Hall conductivity, which can be addressed in the circular dichroism, magnetoluminescence and Faraday rotations, showing distinguishable features from graphene and 2DEG. Our predictions also apply to other group-VI TMDs.

LLs and valley splitting. The monolayers of MoS₂ consist of a Mo layer sandwiched between two S layers in a trigonal prismatic arrangement. Although similar to graphene in many aspects, some of its properties are more favorable than graphene. It features a direct band

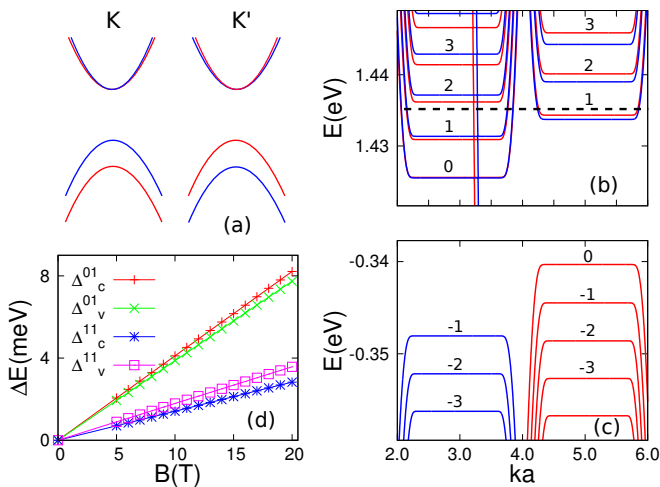


FIG. 1: (color online) (a) schematic of the spin-valley coupled band structure of TMDs. Red(blue) represents spin up(down), respectively. (b) and (c): Conduction and valence band LLs for MoS₂ under $B_{\perp} = 20$ T. K(K') valley is on the left(right). The crossing-LL states in the conduction band are from the dangling bonds on the zigzag edges³⁴, which do not affect the LLs. Dash line is a guide to eye for valley splitting and also marks filling level $\nu(K) = 4$, $\nu(K') = 2$. (d) Δ_c^{01} (Δ_v^{01}) is the absolute energy difference between the LL 0(-1) in K valley and 1(0) in K' valley in conduction(valence) band. $\hbar\omega_0^c$ ($\hbar\omega_0^v$) is the LL spacing in conduction(valence) band. (e) same as (d) calculated from orbital magnetic moment and effective mass approximation. a is the lattice constant.

gap Δ in the visible wavelength regime, which occurs at the two inequivalent valleys K and K' at the corners of the hexagonal Brillouin zone. The inversion symmetry is naturally broken in the monolayers, which induces both strong spin-orbit coupling and spin-valley coupling^{19,20}.

The zero-field band structure for monolayer MoS₂ is schematically shown in Fig. 1(a), which is usually described by the effective Dirac model^{19,20}. In each valley there are two sets of gapped Dirac spectra with red (blue) representing spin up (down) respectively. Because of the large effective mass at the band edges the LLs only scale as $n\hbar e B_{\perp}/m^*$ at the low energy part, which resemble conventional 2D semiconductors more rather than Dirac fermions^{29–33}. Here B_{\perp} is the perpendicular magnetic field and n is the LL index. To obtain the LLs, we adopt a three-band atomic tight-binding model from Ref.³⁴ and apply B_{\perp} via the Peierls substitution $t_{ij} = t_{1,2} e^{-ie/\hbar \int \mathbf{A} \cdot d\mathbf{x}}$, where $\mathbf{A} = (-By, 0, 0)$ is the vector potential.

In Fig. 1(b-c) we present the low energy LLs, where a zigzag ribbon structure is used with a width $L_y = 170$ nm, which is sufficiently larger than the magnetic length l_B . The set of LLs from the lower split-off valence bands are not shown since they are similar to Fig. 1(c). The Zeeman splitting is first neglected here and will be discussed later. We label the LLs and assign the $n = 0$

LLs according to the analytic solutions from the effective two-band Dirac model²⁹. When $B_{\perp} > 0$ they appear only in conduction band of K valley and valence band of K' valley. Therefore the valley degeneracy for them is already lifted. Here our focus is on the more general $n \neq 0$ LLs.

We notice a systematic valley splitting exists for all $n \neq 0$ LLs with the magnitude comparable to the LL spacing, which is not revealed by the effective model²⁹. A linear relation with B_{\perp} is found. Here we let $B_{\perp} \geq 5$ T to ensure $L_y \gg l_B$. The linearity should extend to the low field situation in this single-particle calculation. The linear valley splitting and its discrepancy with the effective model can be intuitively understood from the orbital magnetic moment^{35,36}, which is of opposite sign at the two valleys ($\pm m$). Taking the conduction band as an example, in the presence of B_{\perp} the valley energy difference is $\Delta_c^{01} = 2m \cdot B_{\perp}$. In the effective model, this matches $\hbar\omega_0^c$, the LL spacing between 0 and 1, resulting in valley degeneracy in $n \neq 0$ LLs³⁷. Such matching is violated in the tight-binding model where $\Delta_c^{01} > \hbar\omega_0^c$ giving rise to the valley splitting, as is shown in Fig. 1d and 1e. In the case of graphene, the valley degeneracy is known to be lifted in high magnetic fields via electron-electron or electron-phonon interactions^{38–41}. Similar linear relations between the valley splitting and B_{\perp} have also been experimentally observed in silicon and AlAs 2D electron systems^{42,43}. Their physical origin, however, remains controversial.

The valley splitting here has a few direct consequences: (i) The $n = 0, 1$ LLs in conduction band are always valley polarized and $n = 0, -1$ in valence band are spin-valley polarized. (ii) The total filling factor follows a sequence $\nu = 2, 3, 4, \dots$ in the electron doped regime and $\nu = -1, -2, -3, \dots$ in the hole doped regime. The lifting of valley degeneracy in $n = 0$ LLs can be attributed to the broken spatial-inversion symmetry in the monolayer. Such symmetry is known to guarantee the valley degeneracy rigorously on graphene, regardless of the time-reversal symmetry⁴⁵. However, it does not explain the splitting in $n \neq 0$ LLs⁴⁶. Instead, using graphene lattice as a toy model, we find the splitting in $n \neq 0$ LLs can be induced by the next-nearest-neighbour (NNN) electron hopping, which breaks the electron-hole symmetry. Therefore the valley-splitting in $n \neq 0$ LLs stems from spontaneous breaking of spatial-inversion, electron-hole and time-reversal symmetry. In fact, the low energy physics in MoS₂ is dominated by electron hopping between Mo atoms, which is indeed the NNN hopping on the honeycomb lattice^{19,20}.

Valley-dependent inter-LL selection rules: We now turn to the optical properties of these valley-degeneracy-lifted LLs. Because $\hbar\omega_0 \ll \Delta$, the intraband and interband optical transitions in this system belong to two completely different regimes: intraband in the microwave to terahertz and interband in the visible frequency range. We will set our focus on the latter because for MoS₂ the valley contrasting interband optical transitions have

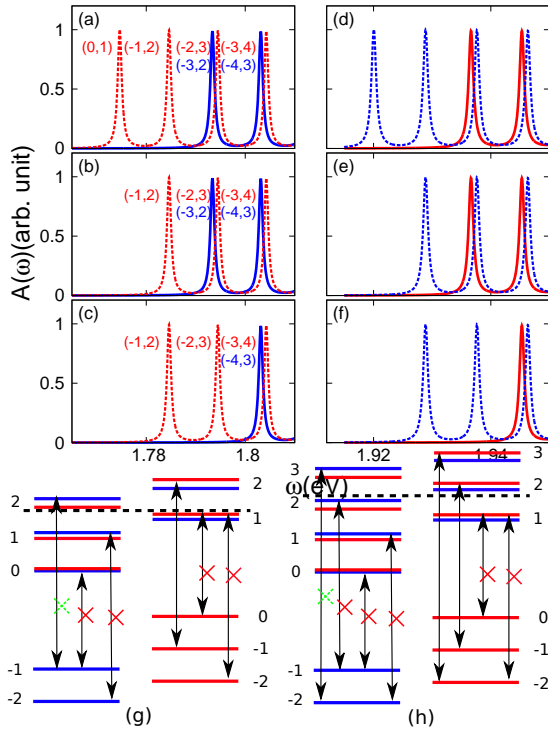


FIG. 2: (color online) Optical absorption spectrum in the quantum Hall regime. The solid(dash) lines represent K(K') valleys, respectively. Red(blue) represents spin up(down), respectively. Spin-valley polarized transitions between (n, n') are labeled. (a)&(d): $\nu(K) = 4, \nu(K') = 0$. (b)&(e): $\nu(K) = 4, \nu(K') = 2$. (c)&(f): $\nu(K) = 6, \nu(K') = 2$. $\Gamma = 0.1\hbar\omega_0$. (g-h) Schematic of the inter-LL transitions corresponding to (b,e) and (c,f). Red(solid) crosses indicate Pauli blocking. Green(dash) crosses indicate vanishing probability.

been the most intriguing property in experiments for valleytronics^{19–24}.

When considering the transitions between levels n' and n , the well-known selection rule for 2DEG and graphene requires $|n| = |n'| \pm 1$ ^{7,8,47,48}. For MoS₂ such selection rule can also be obtained from the effective model⁴⁴. At first glance, since the LL spacing is comparable in the conduction and valence bands, four transitions would occur at very close but non-degenerate photon energies: $-n \leftrightarrow n+1$ and $-(n+1) \leftrightarrow n$ ($n \geq 1$) for both valleys. In Fig. 2 we calculate the optical absorption spectrum

$$A(\omega) \propto \sum_{\epsilon_n < \mu, \epsilon_{n'} > \mu} \frac{|J_x^{nn'}|^2}{i(\epsilon_{n'} - \epsilon_n - \omega - i\Gamma)}, \quad (1)$$

at three different filling levels corresponding to the LLs presented in Fig.1 through exact diagonalization, where J_x is the current matrix and Γ is the broadening parameter. We immediately notice several distinctive features. (i) The expected four-fold peaks only appear two-fold. Unlike in graphene, here the transitions $-n \leftrightarrow n+1$ in K valley and $-(n+1) \leftrightarrow n$ in K' valley are completely

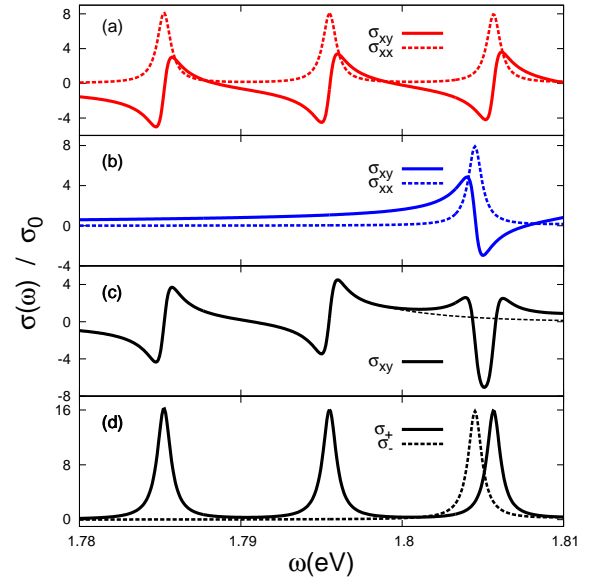


FIG. 3: (color online) Optical Hall conductivity in unit of $\sigma_0 = e^2/h$ with filling factors $\nu(K) = 6, \nu(K') = 2$, corresponding to Fig. 2(c). (a): optical conductivity σ_{xy} and σ_{xx} for spin up, K' valley. (b): spin down, K valley. (c) total σ_{xy} , the dash line schematically shows the cancelling out situation when $\Delta_c^{01} = \Delta_v^{01}$. (d): total $\sigma_{+/-}$. Only the real part is plotted.

suppressed, which suggest highly valley dependent selection rules. Transitions from the spin-split lower valence bands at higher photon energies also follow the same rule except with opposite spins, as seen in Figs. 2(d-f). Such selection rules originate from the severely broken spatial-inversion symmetry in the monolayer. (ii) As the filling level goes up, the number of spin-valley polarized peaks has an alternating $2-1-2-1$ pattern, which can be attributed to the valley-imbalanced Pauli blocking caused by the $n=0$ LLs and the valley splitting as illustrated in Figs. 2(g-h).

To further understand the role played by the valley degree of freedom in the optical Hall effect, we calculate the optical Hall conductivity using the Kubo formula^{14,47,48},

$$\sigma_{ij}(\omega) = \frac{i}{L_x L_y} \sum_{\epsilon_n < \mu, \epsilon_{n'} > \mu} \frac{1}{\epsilon_{n'} - \epsilon_n} \left(\frac{J_i^{nn'} J_j^{n'n}}{\epsilon_{n'} - \epsilon_n - \omega - i\Gamma} - \frac{J_j^{nn'} J_i^{n'n}}{\epsilon_{n'} - \epsilon_n + \omega + i\Gamma} \right), \quad (2)$$

where $i, j = x, y$. Following Ref.⁴⁸, here we retain 40 LLs and impose periodic boundary conditions along the x and y directions. B_{\perp} is kept at 20.8 T, as close as possible to that used Figs. 1 and 2, since in such calculations B_{\perp} can only take discrete levels. The two valleys cannot be distinguished in the momentum space. However, since the valley index is associated with spin, we can distinguish valleys by spins. The result is shown in Fig. 3, where $\sigma_{\pm}(\omega) = \sigma_{xx}(\omega) \pm i\sigma_{xy}(\omega)$ is the optical conductivity for the right and left circular polarized

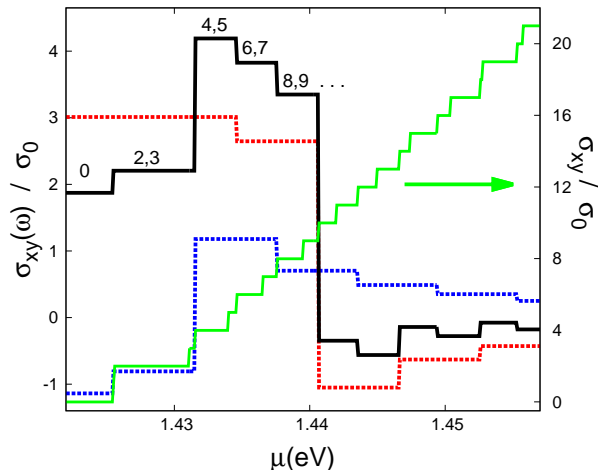


FIG. 4: (color online) Plateau structure for the optical Hall conductivity σ_{xy} (black solid line) at $\omega = 1.786$ eV and the static quantum Hall conductivity (green solid line) in the electron doped regime. Red(blue) dash line represents spin up(down) or K' (K) valley component of σ_{xy} , respectively. Numbers on the solid black line indicate the corresponding quantum Hall conductivity.

light. Spin-valley polarized resonance structures for σ_{xy} is found, similar to Fig. 2. In this set-up, for the electron(hole) doped regime the spin-valley polarization is achieved for the spin up (down) and K' (K) valley, respectively. Upon switching the sign of B_{\perp} the valley and spin polarization also flips. At resonance photon frequencies σ_{xy} from the two valleys actually have the opposite signs. This is another distinctive feature from graphene, in which both valleys contribute equally to the total σ_{xy} ^{13,14}. But due to the difference in Δ_c^{01} and Δ_v^{01} (Fig. 1d), the resonance frequencies in the two valleys are slightly miss-matched, leading to spin-valley mixed resonance peaks in σ_{xy} (starting from the third resonance in Fig. 3c) instead of cancelling out.

A more important message from Fig. 3 when compared with Fig. 2 is that the allowed interband transitions in K and K' valleys are solely attributed to the left and right circular polarized light separately

$$\begin{aligned} K : & \quad -(n+1) \leftrightarrow n, \quad \sigma_- \\ K' : & \quad -n \leftrightarrow n+1, \quad \sigma_+ \end{aligned} \quad (3)$$

where $n \geq 0$. Consequently the circular polarization is directly locked with the valley degree of freedom in optical transitions in the quantum Hall regime. Upon flipping the direction of B_{\perp} , the valley index will switch, *i.e.* $K(\sigma_+)$ and $K'(\sigma_-)$.

Optical Hall plateaus. The optical conductivity as a function of the chemical potential μ is shown in Fig. 4, where ω is slightly away from resonance. The static quantum Hall conductivity is also presented, showing fully valley-degeneracy-lifted and well quantized plateaus. We notice that in the optical conductivity each spin or valley component also develops its own and contrasting

plateaus, although like the net $\sigma_{xy}(\omega)$ they are not quantized either. The $n = 0$ LLs and the valley splitting are manifested in the alternating sequence of the step structures in these two components, which also lead to a unique sequence of filling factors in the net $\sigma_{xy}(\omega)$ plateaus, as labelled in Fig. 4. To be specific, 2,3 spans $n = 0$ to $n = 1$ in K valley and 4,5 $n = 1$ in K to the $n = 1$ in K' valley, and so on. Interestingly, the valley contrasting plateaus persist even when μ is in the band gap, as is seen for the 0 plateau that extends all the way to the valence band top.

Circular dichroism, magnetoluminescence and Faraday rotation. Valley resolved interband optical transitions shown in Fig. 2 are readily detectable by the circular dichroism spectroscopy due to the polarization-valley locking. Given the already excellent photoluminescence of monolayer TMDs in zero-field, magnetoluminescence would be an ideal test of the valley dependent selection rules, in which luminescence between individual LLs in a selected valley can be driven by resonant circular polarized excitations in the Faraday geometry^{1,4,5}. The optical Hall conductivity $\sigma_{xy}(\omega)$ can be measured from the Faraday rotation angle $\theta(\omega)$ ^{13,14,48}. A spin-valley polarized excitation would be indicated by a single maximum absolute slope $|d\theta/d\omega|$ at resonant frequencies as shown in Fig. 3c.

Interplay of valley and spin splitting. The Zeeman splitting is estimated to be much smaller than the valley splitting when we assume an ordinary g-factor for electrons ($g = 2$). The Zeeman spin splitting will slightly enlarge the valley splitting in both the valence and conduction bands with the same magnitude. However, the spin in optical transitions is conserved and the spin-Zeeman field does not change valley-dependent inter-LL transition frequency and selection rules. Additionally, the valence band tops at the K (K') valleys are composed of $m = -2$ ($m = 2$) d -orbitals from the Mo atoms^{19,34}, which induce an additional Zeeman-type splitting term in presence of B_{\perp} . The valley splitting in the valence band is further enlarged by this term. The conduction band bottoms are not affected by this term because they are composed of the $m = 0$ d -orbitals of Mo atom^{19,34}. Accordingly, this additional term induces valley-contrasting frequency shift for the inter-LL transitions at each valley, which will appear as a linear shift against B_{\perp} for each valley in the spectrums of circular dichroism and magnetoluminescence. The valley-dependent inter-LL selection rules remain intact.

To conclude, we have shown that valley splitting exists for all the LLs in monolayer MoS₂ and other TMDs even without considering the interaction effects. Optical transitions in the quantum Hall regime follow valley dependent selection rules controlled by the sign of the magnetic field, which lock the circular polarization and valley degree of freedom together. Finally we propose circular dichroism spectroscopy, magnetoluminescence and Faraday rotation measurements as potential tests for the selection rules as well as the valley splitting. An inter-

esting extension of current study would be the disorder and localization effect in the optical Hall effect, since in this system the mixing of valleys inevitably involves spin flipping, which is distinct from graphene^{30,48}.

Acknowledgements R.C. and C.Z. are supported by ARO (W911NF-12-1-0334), AFOSR (FA9550-13-1-0045), and NSF-PHY (1249293). X.L. and Q.N. are supported by DOE-DMSE (DE-FG03-02ER45958),

NBRPC (2012CB-921300), NSFC (91121004), and the Welch Foundation (F-1255). S. W. and X. X. are supported by US DoE, BES, Division of Materials Sciences and Engineering (de-sc0008145). W. Y is supported by the Croucher Foundation(Croucher Innovation Award), and the RGC and UGC of Hong Kong(HKU705513P,HKU9/CRF/13G,AoE/P-04/08).

-
- * Electronic address: chuanwei.zhang@utdallas.edu
- ¹ S. K. Lyo, E. D. Jones, and J. F. Klem, *Phys. Rev. Lett.* **61**, 2265 (1988).
 - ² I. V. Kukushkin, K. V. Klitzing, and K. Ploog, *Phys. Rev. B* **37**, 8509 (1988).
 - ³ S. R. Andrews, A. S. Plaut, R. T. Harley, and T. M. Kerr, *Phys. Rev.* **8** **41**, 5040 (1990).
 - ⁴ S. I. Gubarev, T. Ruf, M. Cardona, and K. Ploog, *Phys. Rev. B* **48**, 1647 (1993).
 - ⁵ I. V. Kukushkin, R. J. Haug, K. von Klitzing, and K. Ploog, *Phys. Rev. Lett.* **72**, 736 (1994).
 - ⁶ M. L. Sadowski, G. Martinez, M. Potemski, C. Berger, and W. A. deHeer, *Phys. Rev. Lett.* **97**, 266405 (2006).
 - ⁷ V. P. Gusynin, S. G. Sharapov, and J. P. Carbotte, *Phys. Rev. Lett.* **98**, 157402 (2007).
 - ⁸ Z. Jiang *et al*, *Phys. Rev. Lett.* **98**, 197403 (2007).
 - ⁹ R. V. Aguilar *et al*, *Phys. Rev. Lett.* **108**, 087403 (2012).
 - ¹⁰ W. - K. Tse and A. H. MacDonald, *Phys. Rev. B* **82**, 161104(R) (2010).
 - ¹¹ S. Bordacs *et al*, *Phys. Rev. Lett.* **111**, 166403 (2013).
 - ¹² D. S. L. Abergel and Vladimir I. Fal'ko, *Phys. Rev. B* **75**, 155430 (2007).
 - ¹³ I. Crassee *et al*, *Nature Physics* **7**, 48 (2011).
 - ¹⁴ R. Shimano *et al*, *Nature Communications* **4**, 1841 (2013).
 - ¹⁵ P. Kuhne *et al*, *Phys. Rev. Lett.* **111**, 077402 (2013).
 - ¹⁶ K. F. Mak, C. Lee, J. Hone, J. Shan, & T. F. Heinz, *Phys. Rev. Lett.* **105**, 136805 (2010).
 - ¹⁷ Z. Y. Zhu, Y. C. Cheng, and U. Schwingenschlogl, *Phys. Rev. B* **84**, 153402 (2011).
 - ¹⁸ B. Radisavljevic, A. Radenovic, J. Brivio, V. Giacometti, & A. Kis, *Nature Nanotech.* **6**, 147–150 (2011).
 - ¹⁹ D. Xiao, G. Liu, W. Feng, X. Xu, and W. Yao, *Phys. Rev. Lett.* **108**, 196802 (2012).
 - ²⁰ T. Cao *et al*, *Nature Communications* **3**, 887 (2012).
 - ²¹ K. F. Mak, K. He, J. Shan, & T. F. Heinz, *Nature Nanotech.* **7**, 494–498 (2012).
 - ²² H. Zeng, J. Dai, W. Yao, D. Xiao, & X. Cui, *Nature Nanotech.* **7**, 490–493 (2012).
 - ²³ S. Wu, *et al. Nature Phys.* **9**, 149-153 (2013).
 - ²⁴ J. S. Ross, *et al. Nature Commun.* **4**, 1474 (2013).
 - ²⁵ K. S. Novoselov, A. K. Geim, S. V. Morozov, D. Jiang, Y. Zhang, S. V. Dubonos, I. V. Grigorieva, and A. A. Firsov, *Science* **306**, 666 (2004).
 - ²⁶ D. Xiao, W. Yao and Q. Niu, *Phys. Rev. Lett.* **99**, 236809 (2007).
 - ²⁷ A. Rycerz, J. Tworzydło and C. W. J. Beenakker, *Nature Physics* **3**, 172 (2007).
 - ²⁸ D. Gunlycke and C. T. White, *Phys. Rev. Lett.* **106**, 136806 (2011).
 - ²⁹ X. Li, F. Zhang and Q. Niu, *Phys. Rev. Lett.* **110**, 066803(2013).
 - ³⁰ H.-Z. Lu, W. Yao, D. Xiao, and S.-Q. Shen, *Phys. Rev. Lett.* **110**, 016806 (2013).
 - ³¹ H. Rostami, A. G. Moghaddam and R. Asgari, *Phys. Rev. B* **88**, 085440 (2013).
 - ³² A. Kormanyos, V. Zolyomi, N. D. Drummond, P. Rakyta, G. Burkard, and V. I. Falko, *Phys. Rev. B* **88**, 045416 (2013).
 - ³³ Zhou Li and J. P. Carbotte, *Phys. Rev. B* **86**, 205425 (2012).
 - ³⁴ G. Liu, W. Shan, Y. Yao, W. Yao, & D. Xiao, *Phys. Rev. B* **88**, 085433 (2013).
 - ³⁵ M.-C. Chang and Q. Niu, *Phys. Rev. B* **53**, 7010 (1996).
 - ³⁶ A. Kormanyos, V. Zolyomi, N. D. Drummond, and G. Burkard, *Phys. Rev. X* **4**, 011034(2014).
 - ³⁷ T. Cai *et al*, *Phys. Rev. B* **88**, 115140 (2013).
 - ³⁸ Y. Zhang *et al*, *Phys. Rev. Lett.* **96**, 136806 (2006).
 - ³⁹ J. G. Checkelsky, L. Li, and N. P. Ong, *Phys. Rev. Lett.* **100**, 206801 (2008).
 - ⁴⁰ X. Du, I. Skachko, F. Duerr, A. Luican, and E. Y. Andrei, *Nature* **462**, 192 (2009).
 - ⁴¹ A. F. Young *et al*, *Nature Phys.* **8**, 550 (2012).
 - ⁴² S. Goswami *et al*, *Nature Physics* **3**, 41 (2007).
 - ⁴³ Y. P. Shkolnikov, E. P. De Poortere, E. Tutuc, and M. Shayegan, *Phys. Rev. Lett.* **89**, 226805 (2002).
 - ⁴⁴ F. Rose, M. O. Goeribig and F. Piechou, *Phys. Rev. B* **88**, 125438 (2013).
 - ⁴⁵ M. Koshino, E. McCann, *Phys. Rev. B* **81**, 115315 (2010).
 - ⁴⁶ J. N. Fuchs and P. Lederer, *Phys. Rev. Lett.* **98**, 016803 (2007).
 - ⁴⁷ T. Morimoto, Y. Hatsugai, and H. Aoki, *Phys. Rev. B* **78**, 073406 (2008).
 - ⁴⁸ T. Morimoto, Y. Hatsugai, and H. Aoki, *Phys. Rev. Lett.* **103**, 116803 (2009).